Modification of Electron Velocity Distribution in Bounded Plasmas by Secondary Electron Emission

Dmytro Sydorenko, Andrei Smolyakov, Igor Kaganovich, and Yevgeny Raitses

***Abstract*—A particle-in-cell code has been developed for simulations of plasmas of Hall thruster discharges. The simulated system is a plasma slab bounded by dielectric walls with secondary electron emission. An external, accelerating electric field directed parallel to the walls and an external magnetic field directed normal to the walls are applied. The strongly anisotropic non-Maxwellian electron velocity distribution function is obtained in simulations. The average energy of electron motion parallel to the walls is defined by collisional heating in the accelerating electric field. This energy is much higher than the average energy of electron motion normal to the walls, which is determined by the energy of electrons produced in ionization and by scattering of electrons by neutral atoms. The electron distribution function for velocity components normal to the walls is depleted for energies above the near-wall plasma potential. The effects of Coulomb collisions on the electron velocity distribution function and electron wall losses are studied.**

***Index Terms*—Electron beams, electron emission, Hall effect, particle collisions, plasma engines, plasma sheaths.**

I. Introduction

IN CONFINED plasmas, the electron flux to the wall is determined by the electron velocity distribution function (EVDF) and by the sheath potential, which are consistent with the wall properties. It is shown, mostly numerically but also experimentally, that numerous kinds of low-pressure discharges, such as electron cyclotron resonance (ECR) discharges [1], capacitively and inductively coupled plasmas [2]–[4], direct current (dc) discharges [5], etc., have a non-Maxwellian EVDF. However, for the sake of simplicity, the EVDF is often approximated as a Maxwellian, which may lead to misleading results.

For example, the Hall thruster channel has walls made of ceramics with strong secondary electron emission (SEE). For plasma with a Maxwellian EVDF, the flux of electrons to the bounding wall grows considerably with the increase of the electron temperature [6], which is an important factor that limits the electron temperature. The fluid theories based on the assumption that the EVDF is Maxwellian [7]–[10] predict fast electron cooling due to wall losses and saturation of the electron temperature with the growth of the discharge voltage. However, in experiments [11], [12], the electron temperature inside the thruster channel was several times higher than the maximum value for the electron temperature predicted by the fluid theories. Kinetic studies of plasmas in Hall thrusters [13] reveal the depletion of the high energy tail of the EVDF and the reduction of the electron losses to the wall compared with fluid theories. It was shown in [1] for ECR discharges that the EVDF near a wall is far from Maxwellian and is strongly anisotropic in the loss cone. Therefore, the proper analysis of the plasma-wall interaction requires kinetic plasma simulations.

The loss cone in [1], and in this paper, is defined as follows. Electrons with kinetic energy w form a sphere in the velocity phase space. If $w > e\Phi$, where Φ is the plasma potential relative to the wall, then part of these electrons has the energy of motion normal to the wall w_x sufficient to leave the system, i.e., $w_x > e\Phi$. In the velocity phase space the vectors of velocities of these electrons are inside the cone with the tip at the origin and the angle of opening $2\cos^{-1}(\sqrt{e\Phi/w})$. This cone is called the loss cone.

A particle-in-cell (PIC) code has been developed for simulations of a plasma layer immersed in external electric and magnetic fields and bounded by dielectric walls. The PIC code self-consistently resolves in one spatial dimension both the sheath and the plasma bulk regions. The parallel execution of the PIC code on multiple processors allows for the simulation of the evolution of the plasma slab with width of hundreds of Debye lengths over time intervals of the order of several ion transit times. The numerical study of this model reveals a number of kinetic effects that are important for the physics of Hall thrusters [14]–[16]. The present paper is devoted to the formation of the EVDF in Hall discharges.

The paper is organized as follows. In Section II, the simulated model is presented. In Section III, the properties of the non-Maxwellian EVDF are described. In Section IV, the effects of Coulomb collisions on the EVDF are discussed. The major results are summarized in Section V.

II. Description of the Model

Consider the plasma bounded by two infinite parallel dielectric walls capable of producing SEE (see Fig. 1). The x axis is directed normal to the walls, and the system is uniform along the y and z axes. The plasma is immersed in the external constant uniform magnetic field B_x and electric field E_z. The described system is simulated with a parallel electrostatic PIC code that was developed on the basis of a direct implicit algorithm [17], [18] that reduces numerical heating. The code resolves one spatial coordinate x and three velocity components v_x, v_y, and v_z for each particle.

Elastic, excitation, and ionization collisions between electrons and neutral xenon atoms are implemented via a Monte Carlo model of collisions [19]. The neutral gas density is uniform across the plasma and is not changed during simulations.

Manuscript received October 22, 2005; revised January 24, 2006. This work was supported by the U.S. Department of Energy.

D. Sydorenko and A. Smolyakov are with the University of Saskatchewan, Saskatoon, SK S7N 5E2, Canada (e-mail: dms169@mail.usask.ca).

I. Kaganovich and Y. Raitses are with the Princeton Plasma Physics Laboratory, Princeton, NJ 08543-0451 USA.

Digital Object Identifier 10.1109/TPS.2006.875727

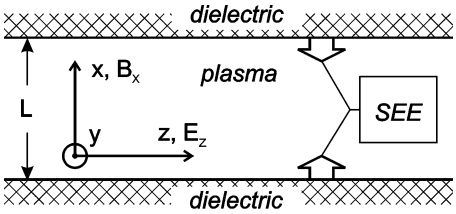

Fig. 1. Schematic diagram of the simulated plasma system. Two dielectric walls represent the coaxial ceramic channel of a Hall thruster.

To account for the anomalously high electron mobility across the magnetic field in Hall thrusters, additional "turbulent" collisions are introduced [8] that randomly scatter particles in the y–z plane without changing their energy [20]. The chosen model of "turbulent" collisions is related with the assumption that in Hall thrusters the anomalous electron mobility is due to their scattering by the fluctuations of the azimuthal electric field [21]. Such scattering occurs in the plane parallel to the bounding walls and does not affect the electron velocity normal to the walls. The electron–electron and electron–ion collisions are implemented via the Langevin formulation described in [22].

The SEE model is similar to that of [23]. The total flux of secondary electrons consists of elastically reflected primary electrons, inelastically backscattered primary electrons, and true secondary electrons. Injection of these components is determined by the corresponding emission coefficients, which are functions of the energy and the angle of incidence of primary electrons [10], [23]–[25]. The ions are neutralized after collision with the wall increasing the surface charge. The total emission coefficient γ agrees with the available experimental data for boron nitride ceramics grade HP [26].

The PIC code was benchmarked against the available numerical and theoretical results. The code reproduces the main results of the early sheath simulations [27] with a Maxwellian plasma source and SEE with a constant emission coefficient (for such simulations, the wall at $x = 0$ is substituted by a plasma source). The linear increments of the two-stream instability of a cold beam in a dense cold plasma [28] and the nonlinear saturation of the beam-plasma instability [29] are reproduced with periodic boundary conditions. The Coulomb collisions model was tested on the problem of maxwellization of the anisotropic "rectangular" EVDF similar to the test simulation described in [22]; the good qualitative and quantitative agreement with the results of [22] was found.

The frequency of "turbulent" collisions was typically obtained as follows. The neutral gas density determined the frequency of electron–neutral collisions $\langle \nu_{en} \rangle$, here $\langle \ldots \rangle$ means averaging over the EVDF. Then the "turbulent" collision frequency ν_t was adjusted such that the electron mobility μ_c due to both "turbulent" and electron–neutral collisions corresponds to the experimental value of the electron electric current density $J_{\exp}$:

$$J_{\exp} = e n_e \mu_c E_z = e n_e \frac{e \nu_{\text{eff}}}{m \left(\nu_{\text{eff}}^2 + \omega_c^2 \right)} E_z \qquad (1)$$

TABLE I
PARAMETERS AND RESULTS OF SIMULATIONS WITHOUT COULOMB COLLISIONS

Number	1	2	3	4
U_d, [V]	300	350	n/a	n/a
E_z, [V/cm]	52	200	200	40
B_x, [G]	91	100	100	100
$\langle w_z \rangle$, [eV]	14.4	24.5	10.8	2.15
$\langle w_x \rangle$, [eV]	4.1	5.75	4.8	1.32
$\widetilde{T}_z$, [eV]	20.1	35.7	22.7	4.2
$\widetilde{T}_x$, [eV]	10.1	12.3	11.8	3.9
Φ, [V]	23	22	20	6.2
$\langle \nu_{en} \rangle$, [10^6s^{-1}]	1.4	1.4	1.4	0.95
$\langle \nu_t \rangle$, [10^6s^{-1}]	7.81	1.46	0	0

where $\nu_{\text{eff}} = \nu_t + \langle \nu_{en} \rangle$ is the effective collision frequency due to both "turbulent" and electron–neutral collisions, $-e$ and m are the electron charge and mass, n_e is the electron density averaged over the width of the plasma slab, ω_c is the electron cyclotron frequency.

As it is described above, the "turbulent" collision frequency is obtained without the effects of plasma-wall interaction on the plasma conductivity. This is a good approximation for simulations of the low-voltage regimes of thruster operation ($U_d \leq 300$ V), when the intensity of secondary electron emission is low and the wall effects are weak. In these regimes the increase of electron mobility due to "turbulent" collisions is the dominating effect. However, simulations with parameters corresponding to high discharge voltages ($U_d \geq 350$ V) reveal that the near-wall conductivity [30] may significantly increase the electron current along the external accelerating electric field (see [31]). In this case, in order to reproduce the experimental current value in simulations, the "turbulent" frequency has to be adjusted according to (1) with $\nu_{\text{eff}} = \nu_t + \langle \nu_{en} \rangle + \nu_{ew}$, where ν_{ew} is the electron-wall collision frequency (which in its turn has to be obtained in simulations). In this paper, we are focused on the parametric study of the effects of "turbulent" collisions on the EVDF rather than on the exact reproduction of the experimental current.

III. PROPERTIES OF THE EVDF

The initial parameters of several simulations with two dielectric walls described in this section are presented in Table I. For all simulations, the width of the plasma slab is $L = 2.5$ cm, the neutral gas density is $n_a = 2 \cdot 10^{12}$ cm^{-3}. Simulations 1–2 were carried out with parameters corresponding to the values experimentally measured in a 2 kW Hall thruster for discharge voltages $U_d = 300$ V and $U_d = 350$ V [32]. In these simulations, the axial electric field E_z and the radial magnetic field B_x were taken at the point of maximal electron temperature, which is inside the thruster channel for the discharge voltage range considered. The initial EVDF is isotropic Maxwellian. As far as Coulomb collisions are typically considered negligible for plasmas of Hall thrusters [33], in simulations described in this section the electron–electron and electron–ion collisions were omitted.

The simulations reveal that the average energy of electron motion along the accelerating electric field $\langle w_z \rangle = \langle mv_z^2/2 \rangle$ is several times larger than the average energy of electron motion normal to the walls $\langle w_x \rangle = \langle mv_x^2/2 \rangle$ (see Table I), where averaging $\langle \ldots \rangle$ is done over all electrons. Additionally, the average energy of electron motion in y direction $\langle w_y \rangle = \langle mv_y^2/2 \rangle$ exceeds $\langle w_z \rangle$ by the value related with the $E \times B$ drift motion. Thus, the EVDF is strongly anisotropic. Regardless of the $E \times B$ drift, the difference between velocity distributions over v_z and v_y is minor and only the EVDFs for v_x and v_z are discussed below.

Qualitatively, the anisotropy of the EVDF can be explained as follows. The electrons gain their energy from the accelerating electric field E_z as a result of "turbulent" collisions and collisions with neutral atoms. Every collided electron gains its average energy when the guiding center of the electron cyclotron orbit displaces against the electric field during approximately half of the period of cyclotron rotation *after* the scattering occurred. The field E_z affects directly only the z velocity and, correspondingly, modifies the energy w_z of an electron. However, the cyclotron rotation distributes this energy between the y and z degrees of freedom. As a result, the heating occurs in the direction parallel to the walls (independent on the particular choice of this direction in the $E \times B$ drift frame), while the electron–neutral collisions strive for making the electron distribution function isotropic [34]. If the frequency of "turbulent" collisions is much higher than the frequency of collisions with atoms

$$\nu_t \gg \nu_{en} \tag{2}$$

the electrons gain energy of motion parallel to the walls much faster than this energy is transferred by electron–neutral collisions to the motion normal to the walls, resulting in the anisotropic EVDF [1], [35]. Case 1 in Table I is characterized by the dominating turbulent conductivity (2), which corresponds to the low voltage regime of thruster operation [32]. The EVDF in this case is presented in Figs. 2 and 3. Note that in Fig. 2(a) and Fig. 3(a), the EVDF is strongly depleted for the energies w_x above the plasma potential $w_x > e\Phi(x)$, i.e., in the loss cone [36]. This occurs because the mean free path between two consecutive electron–neutral collisions (which may scatter an electron towards the wall) $\lambda_c \sim 1$ m is much larger than the width of the plasma slab, i.e., $\lambda_c \gg L$. In different energy regions, the EVDF may be approximated by a Maxwellian EVDF with the corresponding temperature. For instance, the EVDF over normal velocity $f_x(v_x)$ obtained by averaging of the three-dimensional (3-D) EVDF $f(v_x, v_y, v_z)$ is characterized by the effective "normal" temperature T_x defined as

$$T_x(w_x) = -\left[\frac{\partial \ln f_x(v_x)}{\partial w_x}\right]^{-1} \tag{3}$$

where $f_x(v_x) = \int_{-\infty}^{\infty}\int_{-\infty}^{\infty} dv_y dv_z f(v_x, v_y, v_z)$. If f_x is not a Maxwellian EVDF, the temperature T_x is a function of the normal energy w_x. It is instructive to introduce the average temperature as follows:

$$(\widetilde{T}_x)^{-1} = \int_0^{\widetilde{w}_x} dw_x T_x(w_x) \left(\int_0^{\widetilde{w}_x} dw_x\right)^{-1} \tag{4}$$

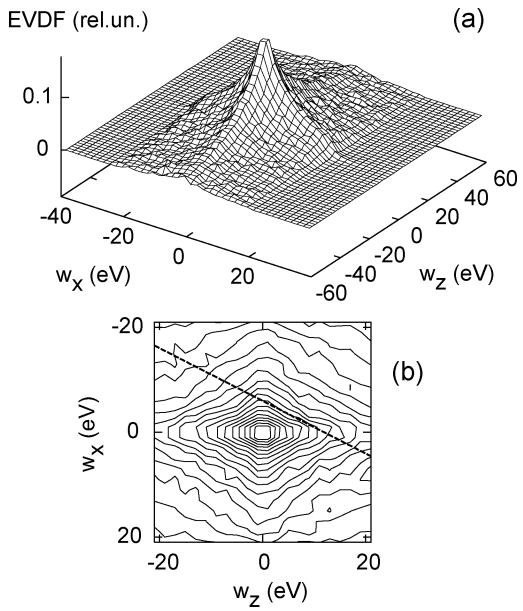

Fig. 2. For case 1 from Table I, the electron velocity distribution over v_x and v_z in the middle of the plasma 10 mm $< x <$ 15 mm plotted in energy coordinates (the sign marks the velocity direction). (a) 3-D-plot. (b) Corresponding 2-D-plot of the low-energy region $|w_{x,z}| < 20$ eV with contour lines. Any two neighboring contour lines in (b) have level difference of 0.01. Plasma potential relative to the wall is $\Phi = 23$ V. Dashed bold line in (b) is $w_x = w_z \widetilde{T}_x/\widetilde{T}_z + const$.

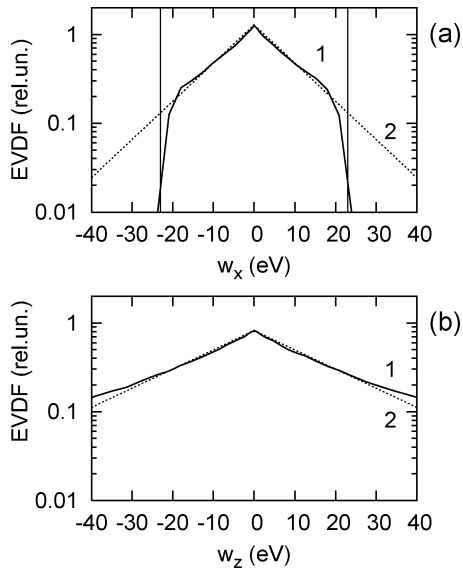

Fig. 3. For case 1 from Table I, the EVDF over v_x (a) and v_z (b) in the middle of the plasma 10 mm $< x <$ 15 mm plotted versus energy coordinate (the sign marks the velocity direction). On both figures curve 1 is the plasma EVDF in simulations. In (a), the two symmetric vertical lines mark the confinement threshold energy $w_x = e\Phi$, straight line 2 has the slope corresponding to $\widetilde{T}_x = 10.1$ eV. In (b), straight line 2 has the slope corresponding to $\widetilde{T}_z = 20.1$ eV.

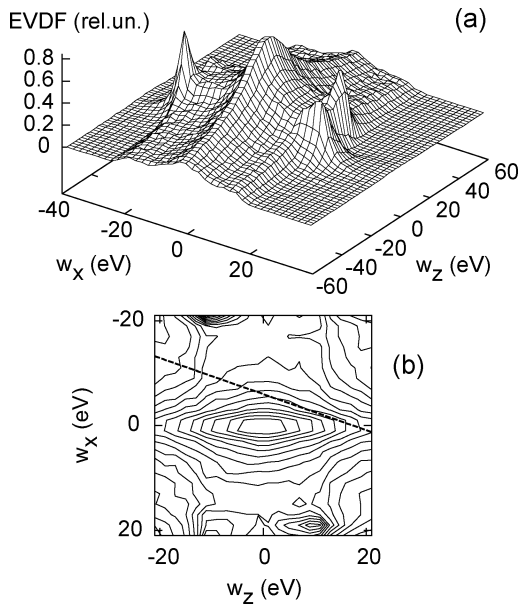

Fig. 4. For case 2 from Table I, the electron velocity distribution over v_x and v_z in the middle of the plasma 10 mm $< x <$ 15 mm plotted in energy coordinates (the sign marks the velocity direction). (a) 3-D-plot. (b) Corresponding 2-D-plot of the low-energy region $|w_{x,z}| < 20$ eV with contour lines. Any two neighboring contour lines in (b) have level difference of 0.05. Plasma potential relative to the wall is $\Phi = 22$ V. Dashed bold line in (b) is $w_x = w_z\widetilde{T}_x/\widetilde{T}_z + const$.

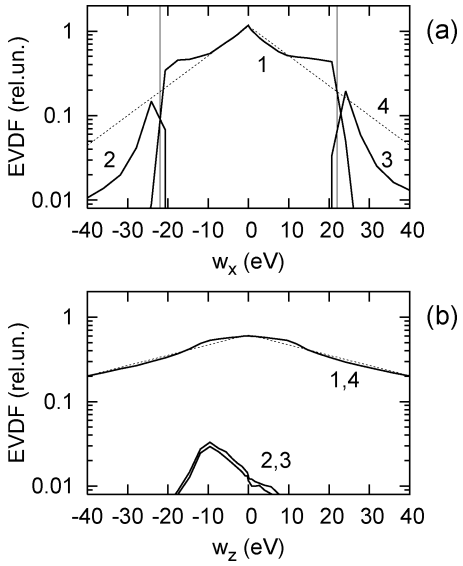

Fig. 5. For case 2 from Table I, the EVDF over v_x (a) and v_z (b) in the middle of the plasma 10 mm $< x <$ 15 mm plotted versus energy coordinate (the sign marks the velocity direction). On both figures, curve 1 corresponds to the bulk electrons; curve 2 to the electron beam emitted from the top wall; curve 3 to the electron beam emitted from the bottom wall. In (a), the two symmetric vertical lines mark the confinement threshold energy $w_x = e\Phi$, straight line 4 has the slope corresponding to $\widetilde{T}_x = 12.3$ eV. In (b), straight line 4 has the slope corresponding to $\widetilde{T}_z = 35.7$ eV.

where the upper integration limit $\widetilde{w}_x$ is chosen such that the EVDF $f_x(\sqrt{2\widetilde{w}_x/m})$ decreases e times compared to the maximum $f_x(0)$, here $e = 2.71828\ldots$. Integration of (4) with (3) gives

$$\widetilde{T}_x = \widetilde{w}_x.$$

Similarly, the effective average temperature in the z direction $\widetilde{T}_z$ may be introduced as the energy value decreasing e times the EVDF over the z velocity $f_z(v_z) = \int_{-\infty}^{\infty}\int_{-\infty}^{\infty} dv_y dv_z f(v_x, v_y, v_z)$, here $e = 2.71828\ldots$.

The ratio between the average temperatures $\widetilde{T}_x$ and $\widetilde{T}_z$ is a better characteristic of the EVDF anisotropy than the ratio of the average energies $\langle w_x\rangle$ and $\langle w_z\rangle$, (see the description of case 4 below in this paper). For a two-dimensional (2-D) EVDF $f_{xz}(v_x, v_z) = \int_{-\infty}^{\infty} dv_y f(v_x, v_y, v_z)$, the contour lines $f_{xz}(v_x, v_z) = const$ form rhombi if the EVDF is Maxwellian; the ratio of the diagonals of a rhombus is the ratio of temperatures. The contour lines of the 2-D EVDF obtained in simulations [e.g., Fig. 2(b)] are similar to rhombi, the linear graph $w_x = w_z\widetilde{T}_x/\widetilde{T}_z + \mathrm{const}$ [see the bold dashed line in Fig. 2(b)] is parallel to the corresponding segments of the contour lines of the EVDF; the smaller the slope of the linear graph—the stronger the anisotropy. The difference from the rhombic shape is due to the finite number of velocity boxes used to calculate the EVDF during simulations.

For high discharge voltages, the difference between the classical and the anomalous axial electron mobility decreases [11] so that $\nu_{tu} \sim \nu_{en}$. In this case, the anisotropy may develop if the axial electric field E_z satisfies the criterion

$$eE_z r_L > e\Phi \tag{5}$$

where r_L is the electron Larmor radius. If criterion (5) is satisfied, the first collision of a low energy electron $mv^2/2 < e\Phi$ provides the electron with a significant energy of motion parallel to the walls $\Delta w > e\Phi$, therefore, the subsequent electron–neutral collision may scatter this electron to the loss cone and the isotropization does not occur. The corresponding simulation is number 2 in Table I. The 3-D-plot of the anisotropic EVDF of such low-collisional plasma is presented in Fig. 4. Note that in the loss cone the structure of the EVDF changes abruptly. This happens because the loss cone is populated not only by the scattered plasma bulk electrons, but also by secondary electrons emitted from the walls. In Fig. 5(a), the corresponding EVDF over v_x is plotted with separated contributions of the secondary electrons and of the plasma bulk electrons. The secondary electrons form two counter-propagating beams [see curves 2 and 3 in Fig. 5(a)], which travel between the walls almost without collisions. The secondary electron beams may form the major part of the EVDF for $w_x > e\Phi$, and, therefore, the main part of the current to the walls. The EVDFs over v_z of the beams of emitted electrons may be locally nonsymmetric, as it is seen in Fig. 4(a) and Fig. 5(b). This asymmetry reflects the motion of the emitted electrons along the spiral-like trajectories: the acceleration and deceleration in x direction is combined with the cyclotron rotation in y–z plane and $E_z \times B_x$ drift in y direction. As a result of this motion at the time of collision with the wall, the average energy of beam electrons exceeds the initial average energy of

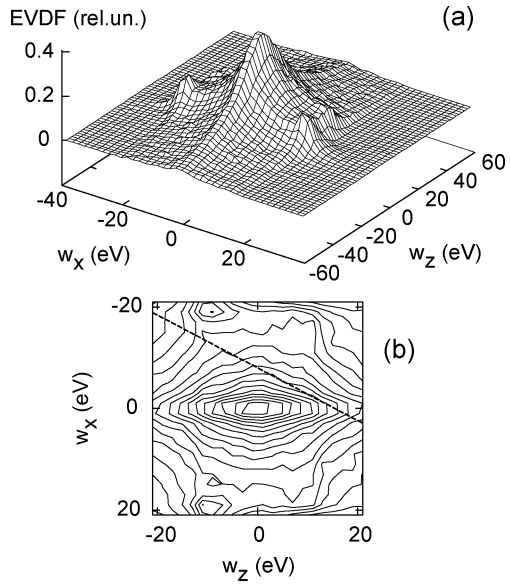

Fig. 6. For case 3 from Table I, the electron velocity distribution over v_x and v_z in the middle of the plasma 10 mm $< x <$ 15 mm plotted in energy coordinates (the sign marks the velocity direction). (a) 3-D-plot. (b) Corresponding 2-D-plot of the low-energy region $|w_{x,z}| < 20$ eV with contour lines. Any two neighboring contour lines in (b) have level difference of 0.025. Plasma potential relative to the wall is $\Phi = 20$ V. Dashed bold line in (b) is $w_x = w_z \widetilde{T}_x/\widetilde{T}_z + const$.

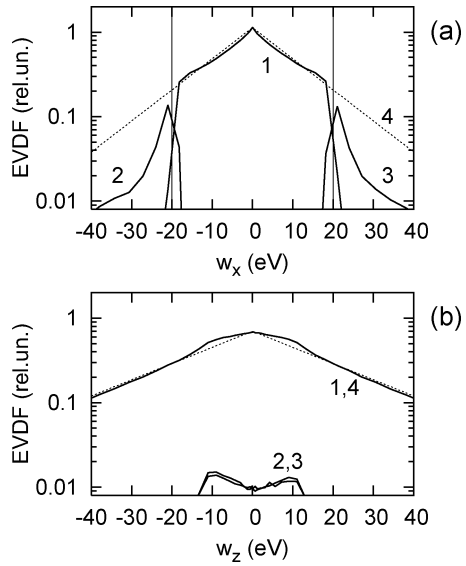

Fig. 7. For case 3 from Table I, the EVDF over v_x (a) and v_z (b) in the middle of the plasma 10 mm $< x <$ 15 mm plotted versus energy coordinate (the sign marks the velocity direction). On both figures curve 1 corresponds to the bulk electrons; curve 2 to the electron beam emitted from the top wall; curve 3 to the electron beam emitted from the bottom wall. In (a), the two symmetric vertical lines mark the confinement threshold energy $w_x = e\Phi$, straight line 4 has the slope corresponding to $\widetilde{T}_x = 11.8$ eV. In (b), straight line 4 has the slope corresponding to $\widetilde{T}_z = 22.7$ eV.

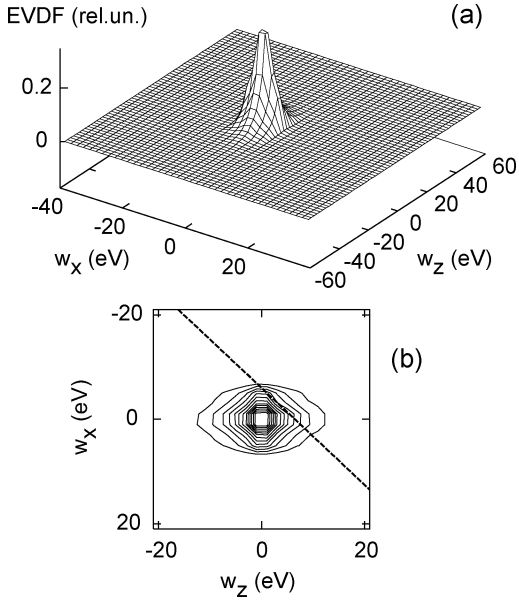

Fig. 8. For case 4 from Table I, the electron velocity distribution over v_x and v_z in the middle of the plasma 10 mm $< x <$ 15 mm plotted in energy coordinates (the sign marks the velocity direction). (a) 3-D-plot. (b) Corresponding 2D-plot of the low-energy region $|w_{x,z}| < 20$ eV with contour lines. Any two neighboring contour lines in (b) have level difference of 0.025. Plasma potential relative to the wall is $\Phi = 6.2$ V. Dashed bold line in (b) $w_x = w_z \widetilde{T}_x/\widetilde{T}_z + const$.

emission by the value of the order of $m(E_z/B_x)^2$ due to the drift motion, which may cause the significant secondary electron emission [31].

In fact, if criterion (5) is satisfied, the anisotropy develops even in the absence of the "turbulent" collisions, as it is proved by simulation 3, see Table I and Fig. 6 with Fig. 7. Note that the anisotropy decreased compared to the case 2, where the turbulent collision frequency was nonzero [compare the slopes of the bold dashed lines in Fig. 4(b) and Fig. 6(b)]. As one can see in Fig. 7, the beams of secondary electrons form the major part of the loss-cone electrons.

When criteria (2) and (3) are not satisfied, like it is for simulation 4 presented in Table I, the anisotropy practically disappears. The difference in the average energies $\langle w_x \rangle$ and $\langle w_z \rangle$ (see Table I) is determined mostly by the strong depletion of the EVDF over v_x in the loss cone [see Fig. 8(a) and Fig. 9(a)]. At the same time for energies below the plasma potential $w_{x,z} < e\Phi$ the distributions over normal velocity v_x and parallel velocity v_z are characterized by very close values of the effective temperatures $\widetilde{T}_x \simeq \widetilde{T}_z$.

Qualitatively, the average parallel electron energy is determined by the balance of Joule heating and wall losses. Thus, the average parallel energy should be proportional to the squared accelerating electric field with some collisional factor. The low average normal energy may be largely determined by the energy of electrons produced in ionization collisions. The correct solution of the problem of scaling of the anisotropy in simulated systems demands an analytical kinetic approach involving calculation of cumbersome collisional integrals. This is the subject of another paper.

IV. Effects of Coulomb Collisions

Scattering of charged particles by Coulomb forces [37] is a basic physical process, important for many phenomena in space plasmas [38], [39] and laboratory plasmas [40], [41]. Coulomb collisions between particles of the same species, e.g.,

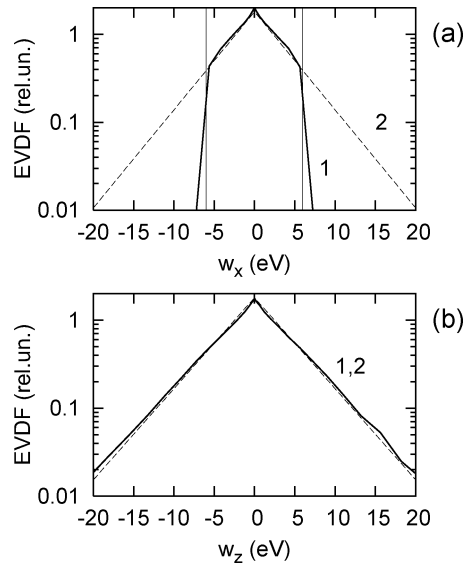

Fig. 9. For case 4 from Table I, the EVDF over v_x (a) and v_z (b) in the middle of the plasma 10 mm $< x <$ 15 mm plotted versus energy coordinate (the sign marks the velocity direction). On both figures, curve 1 is the plasma EVDF in simulations. In (a), the two symmetric vertical lines mark the confinement threshold energy $w_x = e\Phi$, straight line 2 has the slope corresponding to $\widetilde{T}_x = 3.9$ eV. In (b), straight line 2 has the slope corresponding to $\widetilde{T}_z = 4.2$ eV.

electron–electron (e–e) collisions, drive the velocity distribution function towards an isotropic Maxwellian distribution. Coulomb collisions between particles with essentially different masses, e.g., electron–ion (e–i) collisions, are characterized by negligible energy exchange and thus contribute only to the isotropization of the velocity distribution function of light particles. In bounded plasmas, Coulomb collisions supply electrons to the loss cone and thus play the role similar to the role of collisions with neutral atoms. Coulomb scattering occurs predominantly with small angles. Although scattering with large angles $\theta > \pi/2$ is infrequent, many successive small-angle collisions lead to large-angle scattering. For e-i collisions, the effective frequency of large-angle ($\theta = \pi/2$) deflection after many small-angle collisions ν_{ei}^{dif} is given by [42], [43]

$$\nu_{ei}^{dif} = \frac{n_g v e^4 \ln\Lambda}{2\pi^3 \epsilon_0^2 w^2}$$

where n_g is the density of target particles (ions), $w = mv^2/2$ is the electron kinetic energy, v is the electron velocity, $\ln\Lambda$ is the Coulomb logarithm, $\epsilon_0 = 8.85 \times 10^{-12}$ F/m. The frequency of single large-angle collisions ν_{ei}^{sgl} is much smaller than the effective frequency of diffusive deflection ν_{ei}^{dif}, $\nu_{ei}^{sgl} = (\pi^2/32\ln\Lambda)\nu_{ei}^{dif} \ll \nu_{ei}^{dif}$ [42]. The difference between the frequencies of large-angle deflection due to e–i and e–e collisions, ν_{ei}^{dif} and ν_{ee}^{dif}, is a factor of order unity [44]. The effective total frequency of large-angle diffusive deflection ν_{90}^{dif} and the effective total frequency of single large-angle scattering ν_{90}^{sgl} due to both e–i and e–e collisions are

$$\nu_{90}^{dif} = \nu_{ee}^{dif} + \nu_{ei}^{dif} \approx 2\nu_{ei}^{dif}$$
$$\nu_{90}^{sgl} \approx \frac{\pi^2}{32\ln\Lambda}\nu_{90}^{dif}. \quad (6)$$

It is commonly accepted that Coulomb collisions play a minor role [33] in Hall thrusters, for since for such plasmas the frequencies of Coulomb collision ($\nu_{90}^{dif} \sim 10^5$ s^{-1} and $\nu_{90}^{sgl} \sim 10^3$ s^{-1}) are much smaller than the frequencies of electron–neutral ($\nu_{en} \sim 10^6$ s^{-1}) or "turbulent" ($\nu_t \sim 10^6/10^7$ s^{-1}) collisions. The direct modification of the number of particles in the loss cone due to the large-angle Coulomb collisions is about $\nu_{90}^{sgl}/\nu_{en} \sim 0.001$ of the unmodified value. The effective frequency ν_{90}^{dif} characterizes the rate of isotropization of EVDF due to Coulomb collisions, and it can be responsible for filling the loss cone with modification of order $\nu_{90}^{dif}/\nu_{en} \sim 0.1$. The role of Coulomb collisions for electron heating is small, as long as $(\nu_t + \nu_{en}) \gg \nu_{90}^{dif}$, and an electron undergoes many "turbulent" or electron–atom collisions before its velocity is deflected by Coulomb collisions.

Note that the collisional frequencies described in the previous paragraph depend crucially on the design and the regime of operation of a thruster. The frequency of electron–atom collisions ν_{en} is proportional to the neutral gas density n_a, which can be decreased either by reducing the neutral gas flow rate (the so-called throttling regime), or by performing ionization in a different section of the device, as it is in the two-stage thrusters [45]. Additionally, ν_{en} can be decreased if gases lighter than xenon are used (such as argon or hydrogen, with smaller cross sections of electron–neutral collisions). Below it will be shown that in some regimes of a conventional thruster, a small modification of the degree of anisotropy $\widetilde{T}_z/\widetilde{T}_x$ due to Coulomb collisions may result in noticeable changes in the intensity of secondary electron emission, plasma potential and wall current. Modification of the EVDF by Coulomb scattering is consistently connected with the modification of the intensity of secondary electron emission. The emission coefficient γ is defined as $\gamma = \Gamma_2/\Gamma_1$, where Γ_2 is the flux of secondary electrons emitted by the dielectric wall, and Γ_1 is the flux of primary electrons bombarding that wall. The closer the γ is to unity, the more sensitive the plasma becomes with respect to small modifications of the EVDF.

To investigate the modification of the EVDF in a Hall thruster by Coulomb collisions, the pairs of simulations with identical initial parameters have been carried out with and without Coulomb collisions. Initial parameters and major results of these simulations are presented in Table II. The width of the plasma slab is $L = 2.5$ cm; the neutral gas density is $n_a = 10^{12}$ cm^{-3}. The gas density was reduced compared to the value used in the previous section to enhance the effect of Coulomb collision, but it is still within the range of experimental parameters. Initial plasma parameters are: the electron density is $n_{e0} = 10^{11}$ cm^{-3}, the EVDF is Maxwellian with the drift velocity E_z/B_x along the y axis with the electron temperature $T_{e0} = 10$ eV. Duration of simulations until the quasi-steady state is 8 μs for cases 5 and 6, and 10 μs for cases 7 and 8.

In Table II, the effective frequencies of Coulomb collisions ν_{90}^{dif} and ν_{90}^{sgl} are calculated via (6) for electrons with energy equal to the threshold of electron confinement $e\Phi$, and $\ln\Lambda = 10$. The frequency of electron-wall collisions for plasma bulk electrons ν_{wp} is defined as $\nu_{wp} = \Gamma_p/n_e L$, where Γ_p is the

TABLE II
PARAMETERS AND RESULTS OF SIMULATIONS FOR STUDYING THE EFFECTS OF COULOMB COLLISIONS

Number	5	6	7	8
E_z, [V/cm]	50	50	200	200
B_x, [G]	100	100	100	100
Coulomb collisions	off	on	off	on
$\langle w_z \rangle$, [eV]	7.5	7.0	26.8	23.2
$\langle w_x \rangle$, [eV]	1.9	2.2	4.5	4.9
$\widetilde{T}_z$, [eV]	11.7	11.0	36.7	33.5
$\widetilde{T}_x$, [eV]	6.3	6.6	12.1	14.9
Φ, [V]	8.6	11.8	19.4	19.7
$\langle \nu_{en} \rangle$, [10^6 s^{-1}]	0.66	0.66	0.7	0.7
$\langle \nu_t \rangle$, [10^6 s^{-1}]	2.0	2.0	0.7	0.7
ν_{90}^{dif}, [10^6 s^{-1}]	n/a	0.09	n/a	0.08
ν_{90}^{sgl}, [10^6 s^{-1}]	n/a	0.0028	n/a	0.0024
ν_{wp}, [10^6 s^{-1}]	0.072	0.081	0.219	0.356
n_e, [10^{11} cm^{-3}]	0.59	0.56	1.26	1.1
γ	0.61	0.59	0.957	0.965

electron flux consisting of electrons scattered to the loss cone by collisions with neutral atoms or Coulomb collisions.

The pair of simulations 5 and 6 of Table II is characterized by the low axial electric field E_z and the relatively low frequency of "turbulent" collisions ν_t; the effects of modification of secondary emission are minimal for these simulations. Coulomb collisions, accounted for in simulation 6, resulted in the following (compare cases 5 and 6 of Table II).

- The degree of EVDF anisotropy $\widetilde{T}_z/\widetilde{T}_x$ has decreased from 1.86 to 1.67, i.e., by 10%, the electron temperature $\widetilde{T}_x$ has increased.
- The plasma potential Φ has increased by 37%.
- The emission coefficient, γ, has decreased because a more isotropic EVDF has lower energy of electrons in the loss cone, the decrease is insignificant.
- Due to the higher electron temperature $\widetilde{T}_x$, the flux of particles (ions and electrons) to the wall has increased, in particular, the electron wall collision frequency ν_{wp} has increased by 12.5%.
- The loss cone of the EVDF over v_x for bulk electrons [line with markers in Fig. 10(a)] has been shifted to higher energies corresponding to the increased plasma potential. The transition form EVDF bulk to the loss cone is smoothed.
- The EVDF modifications over v_z are insignificant [see Fig. 10(b)].
- The EVDFs over v_x for secondary electron beams (line with markers in Fig. 10(c) for the beam emitted from the bottom wall) have shifted to higher energies in consistence with the increased plasma potential.
- There is no significant difference between EVDFs over v_z for secondary electron beams in both cases [see Fig. 10(d)].

In simulations 7 and 8 of Table II, the electric field E_z is higher than in cases 5 and 6. The emission coefficient γ is close to unity. In these simulations the frequency of "turbulent" collisions was reduced according to the correction due to the near-wall conductivity effect, as discussed above in the end of Section II. The electron current J_z along the external electric field

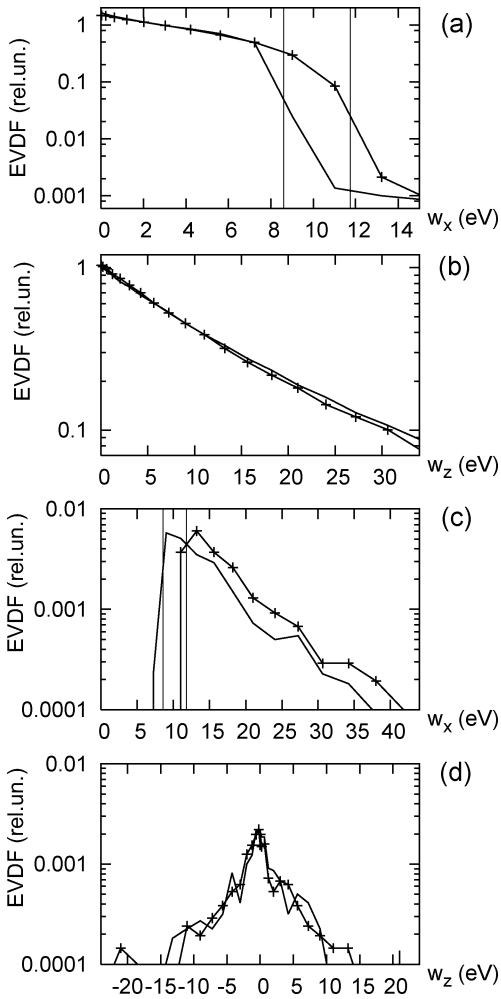

Fig. 10. EVDF over v_x (a) and v_z (b) for the bulk plasma, the EVDF over v_x (c) and v_z (d) for the secondary electron beam emitted from the bottom wall. All EVDFs are plotted versus energy coordinate, the sign marks the velocity direction. Lines without markers correspond to case 5 (Coulomb collisions turned off) and lines with markers correspond to case 6 (Coulomb collisions turned on) from Table II. In (a) and (c), the two vertical lines mark the confinement threshold energies $w_x = e\Phi$ corresponding to cases 5 ($w_x = 8.6$ eV) and 6 ($w_x = 11.8$ eV). EVDFs are calculated in the middle of the plasma $10\,\text{mm} < x < 15$ mm.

corresponds better to the experimental electron current than the current in simulation 2 of Table I carried out with the same external electric field. The Coulomb collisions turned on in simulation 8 resulted in the following difference from simulation 7, as shown in Table II.

- The degree of anisotropy $\widetilde{T}_z/\widetilde{T}_x$ has decreased from 3.03 to 2.25, i.e. by 26%.
- The electron temperature $\widetilde{T}_x$ has increased by 23%.
- The plasma potential has increased insignificantly despite the considerable change in $\widetilde{T}_x$, because the growth of the plasma potential is compensated by the increased intensity of secondary electron emission (see the next item).
- Modification of the plasma potential has resulted in the decreased time of electron flight between the walls, which has lead to the increased energy of secondary electron beam at the target wall [31] and, correspondingly, enhanced the emission coefficient, γ.

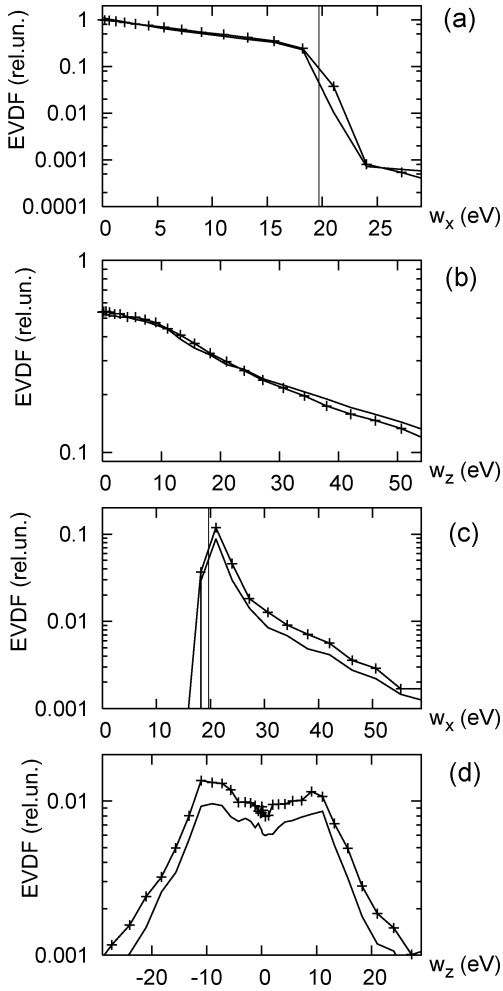

Fig. 11. EVDF over v_x (a) and v_z (b) for the bulk plasma, the EVDF over v_x (c) and v_z (d) for the secondary electron beam emitted from the bottom wall. All EVDFs are plotted versus energy coordinate, the sign marks the velocity direction. Lines without markers correspond to case 7 (Coulomb collisions turned off) and lines with markers correspond to case 8 (Coulomb collisions turned on) from Table II. In (a) and (c), the vertical line $w_x = 19.7$ eV mark the confinement threshold energy $e\Phi$ corresponding to cases 8 (case 7 has a close value $e\Phi = 19.4$ eV). EVDFs are calculated in the middle of the plasma 10 mm $< x <$ 15 mm.

- As far as γ is close to unity, small increase of γ has resulted in significant growth of wall collision frequency ν_{wp}, by 63%.
- The EVDF over v_x for bulk electrons with Coulomb collisions [line with markers in Fig. 11(a)] has smoother transition to the loss cone region and has slightly more particles in this region than the EVDF without Coulomb collisions [plain line in Fig. 11(a)].
- The EVDF over v_z for bulk electrons [line with markers in Fig. 11(b)] has less particles in the high energy tail than such EVDF without Coulomb collisions [plain line in Fig. 11(b)].
- The EVDFs over v_x and v_z for secondary electrons have changed insignificantly, mainly due to the increase of the secondary electron current [see Fig. 11(c) and Fig. 11(d)].

In simulations 5 and 6 the electron energy is lower than in simulations 7 and 8, but the effect of Coulomb collisions is noticeably stronger for the latter case. The reason is the greater sensitivity of plasma parameters to the intensity of secondary electron emission in regimes with $\gamma \approx 1$.

V. Conclusion

The PIC simulations reveal that electron velocity distributions in plasmas of Hall discharges are non-Maxwellian, anisotropic, and depleted for high energies normal to the walls.

The anisotropy is largely determined by high frequency of "turbulent" collisions, which are introduced in order to reproduce the anomalous electron mobility across the magnetic field. However, in the limit of strong external accelerating fields, the anisotropy develops even without "turbulent" collisions. Note that this is in contrast with ordinary gas discharges, where the electron temperature is much smaller and the EVDF is isotropic.

For electrons in Hall thrusters, the frequency of Coulomb collisions is much smaller than the frequency of "turbulent" collisions and collisions with neutral atoms. As a result, the effects of Coulomb collisions on EVDF are typically weak. Considerable changes occur when the secondary electron emission is close to the space charge limited regime, i.e., $\gamma \approx 1$. For typical Hall thruster parameters corresponding to such regime, the electron fluxes to the wall increase by a few tens of percents with Coulomb collisions.

The depletion of the high-energy tail develops because the electron mean free path far exceeds the width of the plasma slab and electrons with energy larger than the plasma potential quickly leave and get lost at the walls. Such region of velocity space forms a loss cone in the phase space. The loss cone may be largely populated by secondary electrons emitted from the bounding walls due to secondary emission. These secondary electrons can considerably contribute to the electron current to the walls and affect the plasma potential. PIC simulations and analytical theory shows that [46] such beams can penetrate plasma from one wall to another. In the limit of complete penetration, the secondary electron flux from one wall is equal to the flux of emitted electrons from another wall. As a result, both fluxes flowing in the opposite directions do not contribute to the electron current, and the space saturated sheath does not occur [16], [47], thus grossly reducing particle wall losses for the bulk plasma compared to the case when the secondary beam penetration is not perfect. The study of electron beam penetration is under way [46].

Acknowledgment

The authors thank A. Smirnov, E. Startsev, and N. J. Fisch for helpful discussions. Simulations were partially carried out using the Westgrid facilities at the University of British Columbia and the University of Calgary. The authors also thank Prof. K. Tanaka for use of the 128-CPU Beowulf-class PC cluster at the University of Saskatchewan, funded by the Canada Foundation for Innovation.

References

[1] I. Kaganovich, M. Misina, S. V. Berezhnoi, and R. Gijbels, "Electron Boltzmann kinetic equation averaged over fast electron bouncing and pitch-angle scattering for fast modeling of electron cyclotron resonance discharge," *Phys. Rev. E*, vol. 61, pp. 1875–1889, 2000.

[2] V. A. Godyak and R. B. Piejak, "Abnormally low electron energy and heating-mode transition in a low-pressure argon rf discharge at 13.56 MHz," *Phys. Rev. Lett.*, vol. 65, pp. 996–999, 1990.

[3] V. A. Godyak and V. I. Kolobov, "Effect of collisionless heating on electron energy distribution in an inductively coupled plasma," *Phys. Rev. Lett.*, vol. 81, pp. 369–372, 1998.
[4] V. A. Godyak, "Nonequilibrium EEDF in gas discharge plasmas," *IEEE Trans. Plasma Sci.*, vol. 34, no. 3, pp. 755–766, Jun. 2006.
[5] R. R. Arslanbekov and A. A. Kudravtsev, "Modeling of nonlocal electron kinetics in a low-pressure afterglow plasma," *Phys. Rev. E*, vol. 58, pp. 7785–7798, 1998.
[6] G. D. Hobbs and J. A. Wesson, "Heat flow through a Langmuir sheath in the presence of electron emission," *Plasma Phys.*, vol. 9, pp. 85–87, 1967.
[7] E. Y. Choueiri, "Fundamental difference between the two Hall thruster variants," *Phys. Plasmas*, vol. 8, pp. 5025–5033, 2001.
[8] M. Keidar, I. D. Boyd, and I. I. Beilis, "Plasma flow and plasma-wall transition in Hall thruster channel," *Phys. Plasmas*, vol. 8, pp. 5315–5322, 2001.
[9] E. Ahedo, J. M. Gallardo, and M. Martinez-Sanchez, "Effects of the radial plasma-wall interaction on the Hall thruster discharge," *Phys. Plasmas*, vol. 10, pp. 3397–3409, 2003.
[10] S. Barral, K. Makowski, Z. Peradzynski, N. Gascon, and M. Dudeck, "Wall material effects in stationary plasma thrusters. II. Near-wall and in-wall conductivity," *Phys. Plasmas*, vol. 10, pp. 4137–4152, 2003.
[11] Y. Raitses, D. Staack, A. Smirnov, and N. J. Fisch, "Space charge saturated sheath regime and electron temperature saturation in Hall thrusters," *Phys. Plasmas*, vol. 12, p. 073507, 2005.
[12] D. Staack, Y. Raitses, and N. J. Fisch, "Temperature gradient in Hall thrusters," *Appl. Phys. Lett.*, vol. 84, pp. 3028–3030, 2004.
[13] N. B. Meezan and M. A. Cappelli, "Kinetic study of wall collisions in a coaxial Hall discharge," *Phys. Rev. E*, vol. 66, p. 036401, 2002.
[14] D. Sydorenko and A. Smolyakov, "Simulation of secondary electron emission effects in a plasma slab in crossed electric and magnetic fields," *Bull. Amer. Phys. Soc.*, vol. 49, p. 261, 2004.
[15] D. Sydorenko, A. Smolyakov, I. Kaganovich, and Y. Raitses, "Modification of electron velocity distribution in bounded plasmas by secondary electron emission," presented at the Workshop Nonlocal Collisionless Phenomena in Plasmas, Princeton Plasma Phys. Lab., Princeton, NJ, Aug. 2–4, 2005..
[16] D. Sydorenko, A. Smolyakov, I. Kaganovich, and Y. Raitses, "Kinetic simulation of effects of secondary electron emission on electron temperature in Hall thrusters," in *Proc. 29th Int. Electric Propulsion Conf.,*, Princeton Univ., Princeton, NJ, Oct. 31–Nov. 4 2005.
[17] A. B. Langdon, B. I. Cohen, and A. Friedman, "Direct implicit large time-step particle simulation of plasmas," *J. Comput. Phys.*, vol. 51, pp. 107–138, 1983.
[18] M. R. Gibbons and D. W. Hewett, "The Darwin direct implicit particle-in-cell (DADIPIC) method for simulation of low frequency plasma phenomena," *J. Comput. Phys.*, vol. 120, pp. 231–247, 1995.
[19] V. Vahedi and M. Surendra, "A Monte Carlo collision model for the particle-in-cell method: applications to argon and oxygen discharges," *Comput. Phys. Commun.*, vol. 87, pp. 179–198, 1995.
[20] A. Smirnov, Y. Raitses, and N. Fisch, "Electron cross-field transport in a low power cylindrical Hall thruster," *Phys. Plasmas*, vol. 11, pp. 4922–4933, 2004.
[21] M. Hirakawa and Y. Arakawa, "Particle simulation of plasma phenomena in Hall thrusters," presented at the Proc. of the 24th International Electric Propulsion Conference, Moscow, Russia, Sep. 1995, IEPC paper 95-164.
[22] W. M. Manheimer, M. Lampe, and G. Joyce, "Langevin representation of Coulomb collisions in pic simulations," *J. Comput. Phys.*, vol. 138, pp. 563–584, 1997.
[23] V. P. Gopinath, J. P. Verboncoeur, and C. K. Birdsall, "Multipactor electron discharge physics using an improved secondary emission model," *Phys. Plasmas*, vol. 5, pp. 1535–1540, 1998.
[24] H. Seiler, "Secondary electron emission in the scanning electron microscope," *J. Appl. Phys.*, vol. 54, pp. R1–R18, 1983.
[25] J. R. M. Vaughan, "A new formula for secondary emission yield," *IEEE Trans. Electron Devices*, vol. 36, no. 9, pp. 1963–1967, Sep. 1989.
[26] A. Dunaevsky, Y. Raitses, and N. J. Fisch, "Secondary electron emission from dielectric materials of a Hall thruster with segmented electrodes," *Phys. Plasmas*, vol. 10, pp. 2574–2577, 2003.
[27] L. A. Schwager, "Effects of secondary and thermionic electron emission on the collector and source sheaths of a finite ion temperature plasma using kinetic theory and numerical simulation," *Phys. Fluids B*, vol. 5, pp. 631–645, 1993.
[28] A. B. Mikhailovskii, *Theory of Plasma Instabilities*. New York: Consultants Bureau, 1974, vol. 1.
[29] N. G. Matsiborko, I. N. Onishchenko, V. D. Shapiro, and V. I. Shevchenko, "On non-linear theory of instability of a mono-energetic electron beam in plasma," *Plasma Phys.*, vol. 14, pp. 591–600, 1972.
[30] A. I. Morozov and V. V. Savel'ev, "Theory of the near-wall conductivity," *Plasma Phys. Rep.*, vol. 27, pp. 570–575, 2001.
[31] D. Sydorenko, A. Smolyakov, I. Kaganovich, and Y. Raitses, "Kinetic simulation of secondary electron emission effects in Hall thrusters," *Phys. Plasmas*, vol. 13, p. 014501, 2006.
[32] Y. Raitses, D. Staack, M. Keidar, and N. J. Fisch, "Electron wall interaction in Hall thrusters," *Phys. Plasmas*, vol. 12, p. 057104, 2005.
[33] J. P. Boeuf and L. Garrigues, "Low frequency oscillations in a stationary plasma thruster," *J. Appl. Phys.*, vol. 84, pp. 3541–3554, 1998.
[34] I. D. Kaganovich and L. D. Tsendin, "The space-time-averaging procedure and modeling of the rf discharge. Part II: Model of collisional low-pressure rf discharge," *IEEE Trans. Plasma Sci.*, vol. 20, no. 2, pp. 66–75, Apr. 1992.
[35] I. Kaganovich, "Modeling of collisionless and kinetic effects in thruster plasmas," in *Proc. 29th Int. Electric Propulsion Conf.*, Princeton, NJ, Oct. 31–Nov. 4 2005, IEPC-2005-096.
[36] L. D. Tsendin, "Energy distribution of electrons in a weakly ionized current-carrying plasma with transverse inhomogeneity," *Sov. Phys. JETP*, vol. 39, p. 805, 1974.
[37] M. Gryzinski, "Two-particle collisions. II. Coulomb collisions in the laboratory system of coordinates," *Phys. Rev. A*, vol. 138, pp. A322–A335, 1965.
[38] C. Y. Ma and D. Summers, "Formation of power-law energy spectra in space plasmas by stochastic acceleration due to whistler-mode waves," *Geophys. Res. Lett.*, vol. 25, pp. 4099–4102, 1998.
[39] B. Abel and R. M. Thorne, "Electron scattering loss in Earth's inner magnetosphere—1. Dominant physical processes," *J. Geophys. Res. Space Phys.*, vol. 103, pp. 2385–2396, 1998.
[40] U. Kortshagen and H. Schluter, "On the influence of Coulomb collisions on the electron-energy distribution function of surface-wave produced argon plasmas," *J. Phys. D*, vol. 25, pp. 644–651, 1992.
[41] A. V. Vasenkov and M. J. Kushner, "Electron energy distributions and anomalous skin depth effects in high-plasma-density inductively coupled discharges," *Phys. Rev. E*, vol. 66, p. 066411, 2002.
[42] M. A. Lieberman and A. J. Lichtenberg, *Principles of Plasma Discharges and Materials Processing*. New York: Wiley, 1994, ch. 3.
[43] L. Spitzer, *Physics of Fully Ionized Gases*. New York: Interscience Publishers, 1962, ch. 5.
[44] R. J. Goldston and P. H. Rutherford, *Introduction to Plasma Physics*. Philadelphia, PA: Inst.Phys., 1995, ch. 11.
[45] A. I. Morozov, A. I. Bugrova, and A. V. Desyatskov *et al.*, "Aton-thruster plasma accelerator," *Plasma Phys. Rep.*, vol. 23, pp. 587–597, 1997.
[46] D. Sydorenko, "Particle-in-cell simulations of electron dynamics in low-pressure discharges with magnetic fields," Ph.D. dissertation, University of Saskatchewan, Saskatchewan, Canada, 2006.
[47] E. Ahedo and F. I. Parra, "Partial trapping of secondary-electron emission in a Hall thruster plasma," *Phys. Plasmas*, vol. 12, p. 073503, 2005.

Dmytro Sydorenko received the M.S. degree from Kharkov State University, Kharkov, Ukraine, in 1993. He is working towards the Ph.D. degree at the University of Saskatchewan, Saskatoon, SK, Canada.

He was a Research Scientist at Kharkov Institute of Physics and Technology, Kharkov, Ukraine. His research interests include particle-in-cell simulation of plasmas of low-pressure discharges, theoretical investigation of the advanced methods of acceleration of charged particles, theoretical study of hybrid (plasma-metal) slow-wave structures.

Andrei Smolyakov received the Ph.D. degree from Moscow Institute of Physics and Technology, Moscow, U.S.S.R., in 1986.

He held a Research Scientist position at the Nuclear Fusion Institute, Russian Research Center "Kurchatov Institute". He is currently a Professor at the Department of Physics and Engineering Physics in the University of Sascatchewan, Saskatoon, SK, Canada. His areas of research include theory of magnetically confined plasmas with applications to controlled thermonuclear fusion and space and astrophysics. He is also interested in low temperature plasma sources for material processing and space propulsion.

Prof. Smolyakov is a Fellow of the American Physical Society and Professional Engineer registered in the province of Saskatchewan.

Igor Kaganovich received the B.S. and M.S. degrees from the Physical–Mechanical Department, St. Petersburg Technical University, St. Petersburg, Russia, and the Ph.D. degree from Ioffe Physical Technical Institute, St. Petersburg, Russia.

He is the Research Physicist at Princeton Plasma Physics Laboratory (PPPL), Princeton, NJ. His professional interests include plasma physics with applications to nuclear fusion (heavy ion fusion), gas discharge modeling, and plasma processing, kinetic theory of plasmas and gases, hydrodynamics, quantum mechanics, nonlinear phenomena, and pattern formation.

Dr. Kaganovich was the recipient of the Alexander von Humboldt Fellowship in 1996. His research was supported by individual grants from international and national funding agencies including DOE, NSF, INTAS, ISF, and RFBR.

Yevgeny Raitses received the Ph.D. degree from the Technion-Israel Institute of Technology, Haifa.

He has been with the Plasma Physics Laboratory, Princeton University, Princeton, NJ, since 1998, where he is currently Research Physicist and the lead scientist on the plasma thruster experiments. Previously, he has held research positions at the Propulsion Physics Laboratory of Soreq NRC, Israel. His current research is focused on plasma–wall interaction in low pressure gas discharges, physics of Hall thrusters, novel plasma and ion sources with applications to satellite propulsion and material processing, and plasma diagnostics.